Applied Surface Science 345 (2015) 109–115

Contents lists available at ScienceDirect

Applied Surface Science

journal homepage: www.elsevier.com/locate/apsusc

The friction coefficient evolution of a TiN coated contact during sliding wear

Guojia Ma[a], Liliang Wang[b,*], Haoxiang Gao[b], Jie Zhang[b], Tom Reddyhoff[b]

[a] Science and Technology on Power Beam Processes Laboratory, Beijing Aeronautical Manufacturing Technology Research Institute, Beijing 100024, China
[b] Department of Mechanical Engineering, Imperial College London, London SW7 2AZ, UK

ARTICLE INFO

Article history:
Received 24 October 2014
Received in revised form 23 March 2015
Accepted 24 March 2015
Available online 31 March 2015

Keywords:
Friction model
TiN coating
Sliding wear

ABSTRACT

This paper discussed the friction coefficient evolution of a TiN coated contact during sliding wear. A hard TiN coating was prepared on a bearing steel (GCr15) substrate by applying the composite method of cathode arc and magnetron sputtering. The microstructure, microhardness, microscratch and tribological behaviour of this coating were studied to obtain the relationship between friction coefficient and other coating properties, meanwhile the full friction coefficient evolution curve with different stages during the wear process of TiN coating was shown. It was found that, coating friction and wear, as two interactive responses from a tribo-system, mutually affected each other and should be studied as a single physical phenomenon. Therefore, a novel friction-wear interactive friction model was developed to represent the evolution of friction coefficient and to predict coating breakdown. The results show that the evolution of the friction coefficient curve can reflect different stages of the wear process and the wear life can be estimated using the new friction model.

1. Introduction

The hard coatings are being widely used in many fields, because of their high hardness, good chemical stability, wear resistance and anti-oxidation capability [1,2], such as the high speed machining and metal forming industries, in which, the coated tools experience inevitable in-service impacts at elevated temperatures with heavy cyclic dynamic loading [3–7]. To understand the interactive responses of the coatings are of great importance not only for the tribological behaviour prediction, but also the research and development of advanced coatings [8,9]. Due to the complex wear mechanisms associated with such coatings, research into their tribological behaviour never ceased. Previous studies [8,9] have focused mainly on the effects of sliding wear and have shown that, for contacts in which either one or both surfaces were coated, four major parameters control in-contact tribological behaviour [10].

These parameters are the coating-to-substrate hardness ratio, the thickness of the coating, the surface roughness and the size and hardness of debris at the contact interface. In addition, these studies also characterised certain tribological properties of the coatings, such as roughness, hardness, ductility, oxide film, reaction layer and adhesive transfer. However, research on the evolution of the friction coefficient of the coating has been lacking, which not only results in a limited understanding of friction and wear processes but also prevents the relationship between control parameters and coefficient of friction being elucidated.

The coefficient of friction is not an intrinsic material property, but instead describes the state of contact between bodies and varies due to the occurrence of wear. In the majority of previous studies on sliding wear of TiN coatings, researches focused on the average value of friction coefficient [8,11–13], with the evolution of friction coefficient being largely ignored. This is surprising since the evolution of friction coefficient indicates different wear stages [14], including the breakdown of the coatings, which is of great benefit to understanding wear mechanisms. A few researchers showed experimental results on the evolution of friction coefficient [15] and the interactive effects between friction and wear, especially, for the tribo-systems with hard coating and lubricant, the breakdown of the coating and (or) lubricant would lead to the typical dual plateau feature in the friction coefficient evolution. However, the coating friction and wear, as two interactive responses from a tribo-system, have not been integrated together and modelled, for instance, Denape and Lamon have already considered interactive effects between friction and wear of available structural ceramics [16], Koji Kato reviewed wear in relation to friction and showed the effects of some major parameters during wear process [9], these findings confirmed that the interactive effect between the friction

* Corresponding author. Tel.: +44 020 758943648; fax: +44 020 75947017.
E-mail addresses: lemontree7678@163.com (G. Ma), liliang.wang@imperial.ac.uk (L. Wang).

http://dx.doi.org/10.1016/j.apsusc.2015.03.156
0169-4332/

and wear does exist and should be studied and modelled jointly and this is the novelty of the present research.

The purpose of this work is to further understand the relationship between wear mechanisms and friction and is achieved by monitoring friction coefficient evolution of a TiN coating contact. Based on these studies, a novel friction model, the interactive friction model, is developed to predict the evolution of the friction coefficient and the wear life of hard coatings.

2. Experimental details

TiN coatings were prepared on bearing steel GCr15 (C: 0.95–1.05, Mn: 0.20–0.40, Si: 0.15–0.35, S: ≤0.020, P: ≤0.027, Cr: 1.30–1.65, Mo: ≤0.10, Ni: ≤0.30, Cu: ≤0.25, Ni + Cu: ≤0.50, the equivalence of AISI52100) substrates by the combination of cathode arc and magnetron sputtering methods. A schematic diagram of the equipment used is shown in Fig. 1. The equipment has four sources including two mid-frequency magnetron sputtering targets and two cathode arc targets, their dimensions being 400 × 120 mm. A rotating workpiece holder is located in the centre of the vacuum chamber. To obtain ions with high energy and plasma with high density, a pulse bias power supply was employed on the holder. To achieve improved TiN coating properties, a heating system is positioned in the vacuum chamber, capable of raising the ambient temperature to approximately 450 °C.

All samples were ground and mirror polished, then cleaned with acetone, dried with hot air and finally fixed onto the substrate holder in the chamber. When the ambient pressure in the vacuum chamber reached 2×10^{-3} Pa, argon gas was introduced and the pressure adjusted to produce a plasma discharge. Undesirable contaminant layers were removed by Ar ion sputter-cleaning for 30 min. Then, two cathode arc targets were turned on, and a Ti transition layer was first deposited on substrate to give an enhanced adherent strength. During this stage, −100 V DC and −500 V pulse composite biases were applied and the deposition time was 5 min. Following this, two mid-frequency magnetron sputtering targets were turned on and nitrogen gas was introduced into the chamber so that a TiN layer was deposited over the Ti transition layer. Other experiment parameters used in TiN coating process are shown in Table 1.

Table 1
Deposition parameters of TiN layer.

N_2 gas flow rate, sccm	500
Working pressure, Pa	0.6
Cathode arc power, kW	2
Mid-frequency magnetron sputtering power, kW	4
Substrate bias (pulse), V	−160
Deposition temperature, °C	350
Deposition time/min	75

A scanning electron microscope (SEM-JEM2010), was used both to characterise the surface morphology of the sample and also to observe the cross-section of the sample in order to measure the thickness of the TiN coating. Three dimensional maps showing the roughness sample prior to testing and the topography of the worn surfaces after testing were measured using a white-light interferometric surface profilometer (NewView™ 7100). The adherent strength of the sample was assessed by a micro-scratch tester (WS-2004) with the maximum load of 50 N and the maximum scratch distance of 5 mm. The micro-hardness of the sample and nano-hardness were evaluated by a micro-hardness tester

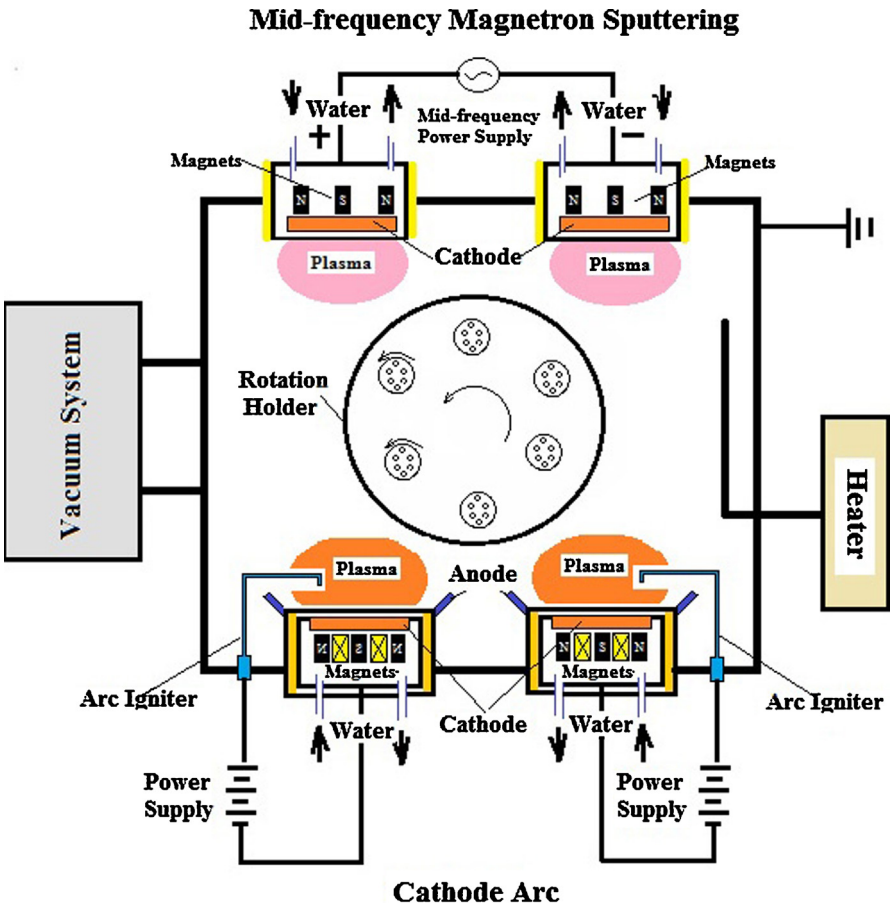

Fig. 1. Schematic diagram of composite cathode arc and magnetron sputtering equipment.

(Woleprt Wilson Instruments – Tukon 2500) with an applied load of 20 N and a nano-hardness indenter (MTS), respectively. The tribological properties of the samples were characterised using a ball on disc tribometer (UMT-2), in which the evolution of friction coefficient, wear rate and wear volume were recorded. A WC-6% Co ball (microhardness 1780 HV, abrasion strength 1380 N/cm, elastic modulus 71 GPa), 6 mm in diameter, was used as the counterpart. All the wear tests were conducted in an ambient environment, at a temperature of 25 °C and a relative humidity of 30%. In the linear tests of the ball on disc, the relative sliding speed was 5 mm/s and the sliding distance was 10 mm.

3. Results and discussions

3.1. Surface morphology, roughness and thickness of the TiN coating

The surface morphology of TiN coating is shown in Fig. 2. Here, it can be seen that the surface is smooth and flat, with only a few visible micro-pores and slight spallation. The mean roughness (R_a) of the TiN coating is 0.10 ± 0.005 μm, measured using the three dimensional optical profilometer, and is very close to R_a of the TiN coating prepared using single magnetron sputtering method [9]. Fig. 2 shows the coated surface with ultra-low roughness, as most of the hard nitride coatings were fabricated by plasma enhanced physical vapour deposition (PEPVD) and plasma enhanced chemical vapour deposition (PECVD). Therefore, the influence of the surface roughness on friction and wear properties was ignored in this study. The cross-section of the TiN coating is shown in Fig. 3, showing a thickness of approximately 2.1 ± 0.05 μm.

3.2. Bonding strength and hardness of the TiN coating

The micro-scratch curve and scratch track morphology of the TiN coating are shown in Fig. 4. By ramping the indenting load, followed by visual examination of the wear track, the critical load which causes the failure of the adhesive bonding can be determined. The scratching process is accompanied by a friction signal (Fig. 4), which exhibits severe fluctuations when the indenting load is greater than a critical value. As shown in Fig. 4, the critical load of the TiN coating is approximately 43.7 ± 0.1 N, suggesting that the bonding strength of TiN coating is sufficient for industrial application. In addition, the micro-hardness of the samples were measured with an applied load of 20 N and the results show that the micro-hardness of the substrate and the TiN coating are 500 ± 8 HV and 622 ± 10 HV, respectively. The strength of the TiN coating was measured by nano-indentation, and the average value of 5 measurements was 32.45 ± 0.43 GPa.

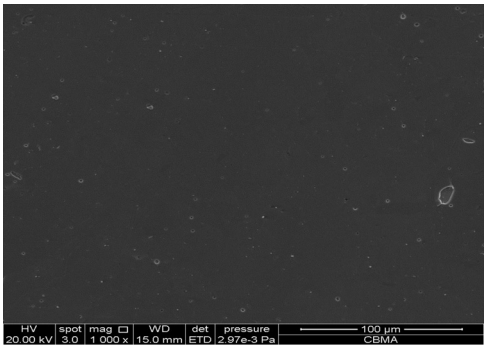

Fig. 2. Surface morphology of the sample.

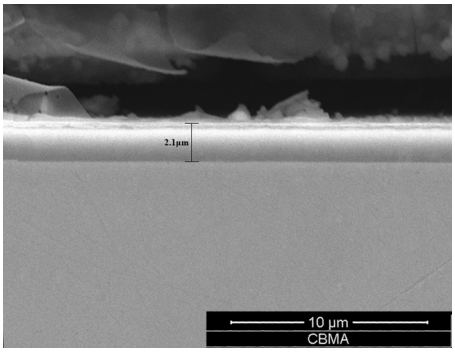

Fig. 3. Cross-section of the sample.

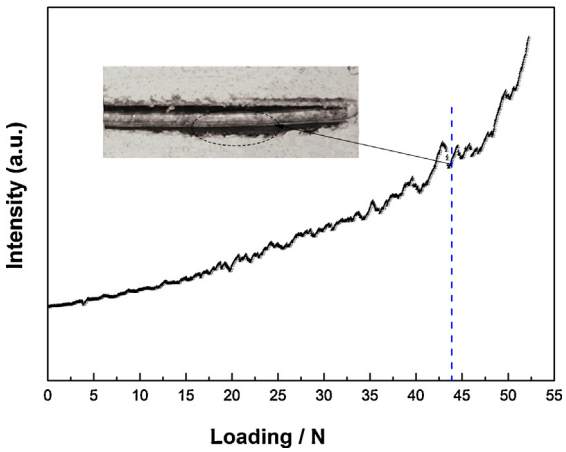

Fig. 4. Micro-scratch curve and scratch track picture of the sample.

3.3. Friction and wear properties of the TiN coating

The friction coefficient evolution of the TiN coating under a normal load of 200 N is shown in Fig. 5. Four interruptions were made during the test so that the wear track could be imaged using an optical microscope. This revealed a varying surface morphology over the entire wear track as shown by the images in Fig. 5 and the microstructural changes shown in Fig. 6. From this data it can be seen that the evolution of friction, can be divided into three stages according to different wear behaviours and mechanisms. These comprise of stage I: low friction stage, stage II: ploughing friction stage and stage III: coating breakdown stage [17,18].

In stage I, the friction coefficient was low and stable, with the value ranging from 0.15 to 0.2. The surface morphology of the wear

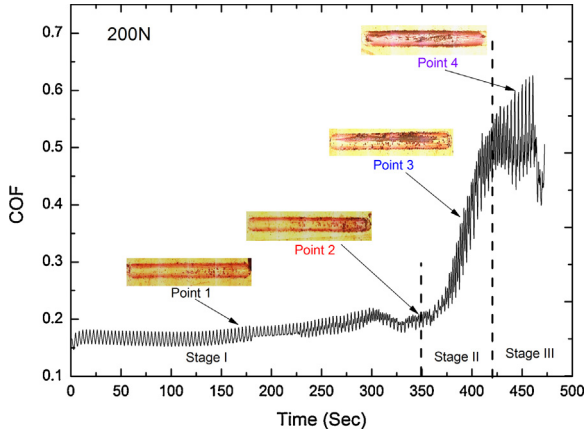

Fig. 5. Friction coefficient evolution of the sample under load of 200 N.

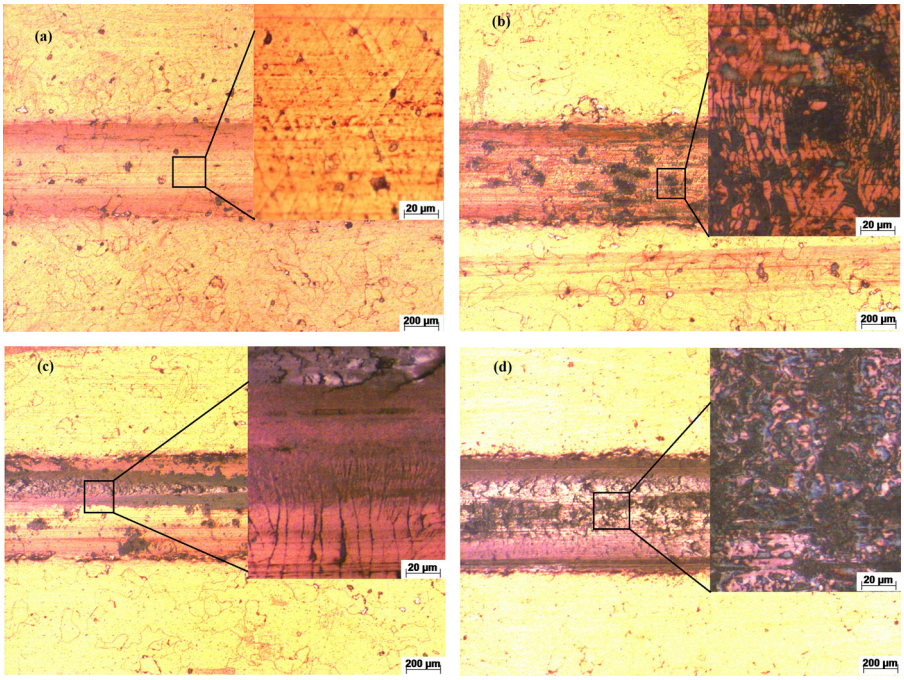

Fig. 6. Wear track pictures of the local enlargement under different time points. (a) 180 s – point 1, (b) 350 s – point 2, (c) 400 s – point 3, (d) 450 s – point 4.

track at wear time of 180 s is shown in Fig. 6(a). Only a small number of micro cracks are visible, but no coating spallation can be observed, thus a negligibly small volume of wear debris was generated during the first half of this stage. As the wear time (sliding distance) increases, further micro cracks developed, and wear debris was generated due to localised coating spallation, as indicated by Fig. 6(b), in which the wear track morphology is shown after a sliding duration of 350 s. The friction coefficient in stage I was primarily generated by the contact between the ball and the coated surface. Here, the friction force stemmed from the ploughing friction arising from the micro surface asperities. The adhesive friction between the ball and the coating was very low and is likely to contribute only slightly to the overall friction. Since the wear debris generated during the initial stage of sliding were loose powder-like and small in size, the ploughing friction caused by the entrapped hard wear particles was very low and negligible interlocking effects occurred. However, at the end of this stage (between 300 and 350 s), the accumulation and entrapment of large wear particles initiated, the increasing quantity (density) and the enlarged size of the wear particles resulted in friction due to third-body hard particles ploughing [19,20] and led to oscillation and rapid increase in the friction coefficient. Therefore, in stage II (after 350 s), the friction coefficient started to rise rapidly from 0.2 to 0.55. These "third body particles" are usually generated in the sliding contact and play a critical role in determining friction [21,22], while their effects depend on their chemical composition and mechanical properties. In the current study, the third body particles were generated from hard TiN debris, which could increase the friction coefficient pronouncedly and accelerate the wear of the coating. The wear track morphology during this stage is shown in Fig. 6(c). Here, the small spallation areas have joined together and developed into local delamination in some areas of the wear track, while the remaining TiN coating with cracks can still be observed in other regions of the wear track. At the end of stage I, loose wear debris must have agglomerated to form larger particles, which – possibly combined with other large particles generated directly from the delaminated wear debris – caused the quantity and size of entrapped wear particles to exceed a critical value. As a result, stage II was dominated by ploughing friction due to role the entrapped high strength wear particles. The wear process then went into severe abrasive wear stage, where the strong dynamic coupling between friction and abrasive wear took place, *i.e.* the friction coefficient increased significantly because of the increasing quantity of entrapped third body particles. On the other hand, the increased friction coefficient resulted in higher shear stresses, which in turn accelerated the wear and the breakdown of the coating. Since the WC-6% Co ball is very hard and has excellent wear resistance, the WC-6% Co ball and TiN hard coating in this study offered very little adhesive friction, which was observed experimentally from the present research and similar results can be found in [23]. Since the occurrence of stick-slip phenomenon depends on the contact materials, particularly, when adhesive friction is the predominant contributor to the overall friction coefficient, thus it was assumed that there was no stick-slip phenomenon during the stages I and II of sliding.

In stage III, the friction coefficient reached a plateau with an average value of 0.6, which is close to that of a typical contact between GCr15 (substrate material) and WC-6% Co ball. In this stage, the ploughing friction due to the third body particles would still play an important role, with the quantity and size of the particles reaching a dynamic balance, *i.e.* the quantity of wear particles entrapped in, and ejected out from, the contact interface being equivalent. In the meanwhile, the ploughing friction between the ball and the GCr15 substrate must have reached a maximum, since the coating has been completely delaminated. In stages II and III, numerous wear particles were generated and these entrapped wear particles could lead to the separation of the contact interface. Due to the nature of ploughing friction, the normal load is taken by the entrapped hard wear particles. The amount of wear particles will affect the real contact area and also the penetration depth of each wear particle, but will not affect the overall ploughing friction. Fig. 6(d) shows that the TiN coating has been completely removed and an oxide layer has formed on the substrate surface. The evidence of the oxide layer formed on the substrate surface can be also found in [14,24]. However, the oxide layer, adhesive debris or abrasive grooves cannot be observed on the surface of the WC-6% Co ball due to its excellent wear resistance and oxidation resistance.

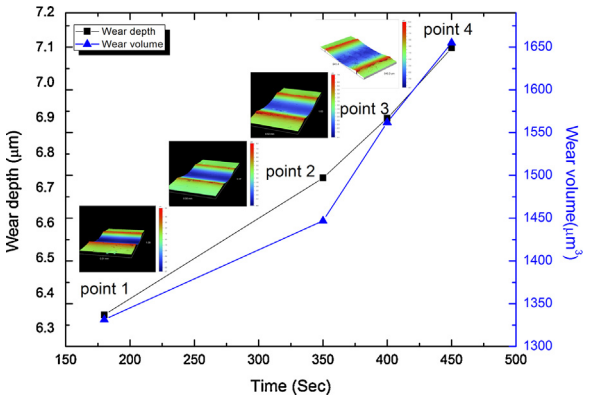

Fig. 7. Wear depth and wear volume of different wear-time points under load of 200 N.

Fig. 7 illustrates the depth and the volume of the wear scar at different stages during the test. A white-light interferometric surface profilometer was used to measure the width and depth of the wear scar to determine the volume of wear. Here, the wear depth and volume increases monotonically with time, however an increased wear rate is observed between points 2 and 4 owing to hard wear particles inducing abrasive wear, with the same trend being observed for the wear volume. Compared with Fig. 3, it was found that the depth of the wear track is greater than the coating thickness, which is due to the severe plastic deformation of the substrate and the coating, indicating that the bonding strength between the coating and substrate was excellent. The enhanced bonding strength was attributed to the Ti sub-layer, although this layer itself is not abrasion resistant and the wear-resistance of the sample will decrease when the TiN layer is removed, because the Ti sub-layer prevents the TiN coating from falling off when initial cracking occurs in the TiN layer. In addition, in Fig. 7, it was found that the width of the wear track has a small change due to a lager deformation and a small wear rate of the sample under the big load.

The effects of normal load on the fiction coefficient are displayed in Fig. 8 for three separate tests. Here, each plot of friction coefficient shows the same evolution again revealing three distinct stages of wear. The duration of stage I decreased significantly with increasing normal load. The friction coefficient of the coating is primary governed by four important factors; coating hardness, coating thickness, surface roughness and entrapped debris [14]. Because the experiments were carried out on the same sample, the difference in friction coefficient between loads must there be attributed to variations in debris behaviour. During stage I, higher normal loads would lead to larger crack lengths and larger sized wear

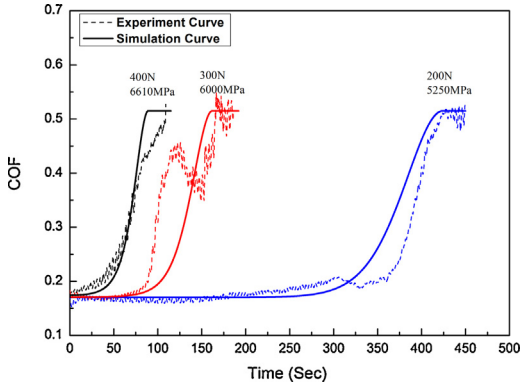

Fig. 8. Simulative and experimental friction coefficient curves of the sample under 200 N, 300 N and 400 N.

particles being generated, which would result in a faster transition from stage I to stage II. In addition to this, the faster wear of the coating under higher normal loads can be explained by the Archard's wear law [25]. In Fig. 8, severe oscillation in the friction coefficient was observed at 300 N – 6000 MPa. The oscillation in the friction test results is a commonly observed phenomenon, because the friction coefficient value is not a material property, which can be affected by many factors. In the present research, this could be caused by the entrapment of large wear particles and the partial breakdown of the coating.

3.4. Interactive friction model

The friction between the WC-6% Co ball and the coating stems from two origins (Eq. (1)) corresponding to two different mechanisms, namely initial friction coefficient μ_α and ploughing friction coefficient μ_{pc}.

$$\mu = \mu_{pc} + \mu_\alpha \tag{1}$$

where μ_α is a friction coefficient representing the initial wear process showing low friction. It was found that the adhesive friction did not play an important role in the present research since the material transfer between the WC-6% Co ball and the coating was very little according to the experimental observations. In the initial low friction stage, wear particles were small in size compared to the height of the asperities, thus the ploughing friction mainly stemmed from the hard asperities, which is represented by μ_α in Eq. (1). The hardness of the WC ball is considered to be much higher than that of the coating, thus the morphology of the hard asperities (on the ball) did not change significantly during the wear process. Therefore, it would be reasonable to assume a constant initial value of friction coefficient $\mu_\alpha \approx 0.17$, which can be determined by running short sliding distance wear tests. In stages II and III, large wear particles were generated as the number of wear particles increased and only the wear particles entrapped between the contact surfaces contributed to the ploughing friction, μ_{pc}, the friction induced by the ploughing of hard wear particles, can be modelled by Eq. (2):

$$\mu_{pc} = \mu_{ps} \exp[-(\lambda_1 h)^{\lambda_2}] \tag{2}$$

where μ_{ps} is ploughing friction of the substrate, λ_1 and λ_2 are model parameters, and h is the instantaneous thickness of the coating. Eq. (2) was developed considering the physical mechanisms of hard wear particles induced ploughing friction. However, to improve the numerical integration efficiency, the equations have been simplified considerably.

The ploughing friction generated from a single spherical shaped wear particle can be estimated by using Eq. (3):

$$\mu_{pc1} = \frac{2\{\sin^{-1}(w/2r) - \{(w/2r)[1-(w/2r)]\}^{1/2}\}}{\pi(w/2r)^2} + \frac{4\{1-[1-(w/2r)^2]^{1/2}\}}{\pi(w/2r)^2}\mu_s \tag{3}$$

where w is the diameter of the indentation (determined by the penetration depth of a wear particle), r is the radius of a wear particle and μ_s is the shear friction coefficient at the particle/coating contact interface. w is determined by the hardness of the two materials in contact and the contact pressure. μ_s is determined by the nature of the mating materials. During the wear process, the normalised wear particle density ρ, entrapped at the contact interface, achieved a dynamic balance between the new generated wear particles (first term in Eq. (4)) and the particles ejected from the wear track

(second term in Eq. (4)), where n_1, n_2, B and C are model constants, and h is the instantaneous coating thickness.

$$\dot{\rho} = B\dot{h}^{n_1}\rho - C\rho^{n_2} \tag{4}$$

The total ploughing friction generated from all the entrapped wear particles is estimated by Eq. (5), (N_{pc} is model parameter) *i.e.* the overall ploughing friction is determined by the normalised wear particle density and the ploughing friction generated from each single entrapped wear particles. However, the ploughing friction (calculated from Eq. (5)) only contribute to the overall friction when the normalised wear particle density ρ is greater than a critical value, representing the entrapment of the large wear particles.

$$\mu_{pc} = N_{pc}\rho^{\lambda}\mu_{pc1} \tag{5}$$

Combining Eqs. (3)–(5) will enable the modelling of the interactive phenomenon of a hard coating tribo-system, although this set of equations requires significant efforts on model parameters calibrations. Therefore, Eq. (2) was developed to simplify the computation procedures. Due to the nature of Eq. (2), the value of μ_{pc} is very low ($\approx$0) over the entire range of stage I to represent the neglectable ploughing friction effect of the wear particles. μ_{pc} started to increase in stage II. This has enabled the modelling of the complex nature of friction and wear in a coating tribo-system, *i.e.* at the very initial stage, the generated wear particles are normally few and small in size, and are therefore unlikely to become entrapped between the asperities and hence contribute negligibly to the ploughing friction. As the wear process continues, the coating's thickness gradually reduces and its load-bearing capability declines. Meanwhile, the number of cracks gradually increases (as shown in Fig. 6(b)), some of which join together to form local delamination (as shown in Fig. 6(c)) and hence results in an increase in the size and number of wear particles. Ploughing friction changes chiefly with the variation of wear particles, and these wear particles are related to the coating thickness, therefore an equation relating ploughing friction to the coating thickness can be built. The instantaneous thickness of the coating in Eq. (2) can be obtained from $h = h_0 - \dot{h}dt$, where h_0 is the initial thickness of the coating, and $\dot{h}$ is the time dependent wear rate of the coating that can be calculated by Eq. (6):

$$\dot{h} = \frac{KPv}{H_c} \tag{6}$$

where K is the coefficient of wear, which is a dimensionless constant, P is the contact pressure, v is the sliding velocity ($v = dl/dt$) and H_c is the combined hardness of the coating and the substrate. This equation is based on Archard's wear equation [25], which is a widely used model to estimate sliding wear. A time-dependent integration algorithm is introduced in the present model, by integrating the amount of wear in each time step/increment to model the evolution of wear occurred in the tribo-system. The benefit of this algorithm is to take the time history of wear into account, *e.g.* if the sliding speed has changed during the wear test, the interactive friction model will, uniquely, adjust the wear rate correspondingly. Although Archard's equation indicates that the volume of the removed debris due to wear is proportional to the friction forces and the material hardness [26], some important factors have not been considered [27,28]. These include the evolution of the coating thickness and combined hardness. During the wear process, the coating thickness decreases leading to a reduction of the combined hardness that, in turn, accelerates the breakdown of the coating. Therefore, Archard's equation should be modified by introducing the combined hardness H_c. To achieve this, the current research applies Korsunsky's model (Eq. (7)) to calculate combined hardness since it has shown good agreements with a wide range of experimental data [29,30],

$$H_c = H_s\left(\frac{\alpha^2 + h\beta^2}{\alpha + h\beta^2}\right) \tag{7}$$

where H_s is the hardness of the substrate, α is the hardness ratio between the coating and the substrate, β is an influence coefficient of the thickness, and h is the instantaneous thickness of the coating. The combined hardness is Vicker's hardness value, a joint response of the coating and substrate, determined by using a Tukon 2500 hardness tester. As indicated by Eq. (7), the combined hardness is determined by the residual thickness and the mechanical property of the coating. Therefore, as the wear test proceeds, the combined hardness reduces correspondingly. When the coating was worn off completely, the combined hardness value was equivalent to the hardness of the substrate material. In the present research, we calibrated the model by interrupting tests, to determine the model parameters in Eq. (6), the Archard's wear law, and to ensure that the predicted residual coating thickness to follow the experimental results. In addition, the wear model integrated in the interactive friction model offers sufficient flexibility to describe different trends of wear, *e.g.* a parabola or linear trend *etc.*

The overall interactive, mechanism-based, model used in this study combines Eqs. (1), (2), (6) and (7). P, v, H_s, and μ_α are initial conditions of friction model for TiN sample. Throughout the numerical analysis, μ_{p_s}, α, λ_2 and β are load independent parameters, while λ_1 and K are load dependent parameters. Those load dependent parameters can be represented by the following Power Law equations (Eqs. (8) and (9)):

$$\lambda_1 = k_{\lambda_1}P^{N_{\lambda_1}} \tag{8}$$

$$K = k_K P^{N_K} \tag{9}$$

where P is the pressure load applied, and k_{λ_1}, k_K, N_{λ_1}, and N_K are material constants. μ_{p_s} and μ_α are determined by the friction coefficient at the initial and final stage of testing. N_k, N_{λ_1}, k_{λ_1}, λ_2, α and k_K values can be determined from the friction evolution curves.

The friction model was calibrated using the experimental data from the tests carried out under three different loads shown in Fig. 8. In order to optimise the interactive friction model, the material constants were determined between the numerical simulation and experimental data. The resulting material constants along with certain model parameters used in the interactive friction model are listed in Table 2. Once the parameters and constants have been determined in this way, the model can be used to predict the evolution of friction coefficient under different loads. This approach has been verified and the results shown in Fig. 9, where simulative and experimental fiction coefficient curves are compared from two new tests (without recalibration of the model) presented, indicating that the interactive friction model developed in the present research enables the prediction of friction coefficient evolutions within the boundaries for calibration, *i.e.* between 200 and 400 N in the present research. It is evident that the simulation curves agree closely with the experimental results. Furthermore, the simulation curve includes three stages; a low friction stage, a debris friction stage and a coating failure stage. The evolution of friction coefficient featured by the three-stage pattern (or the double plateau pattern),

Table 2
Material constants and model parameters of interactive friction model for TiN layer.

λ_2	μ_{p_s}	N_{λ_1}	N_k
2	0.311	−3.84	4.095
α	k_{λ_1}	k_K	μ_α
6	4.58E17	7.27E-23	0.17

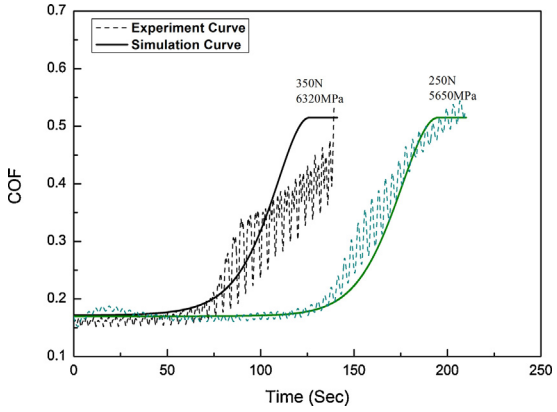

Fig. 9. Simulative and experimental fiction coefficient curves of the sample under 250 N and 350 N.

due to the breakdown of the coating, is very widely observed in the hard-coating tribo-system. Theoretically, these features can be modelled by the interactive friction model, by the re-calibration of the model parameters. With that said, it should be recognised that this study is preliminary and requires further experiments on different types of hard coating in order to optimise the model. In addition, since the model is based on wear tests of short duration, the influence of the oxide as a third body has been ignored. However, oxide is often generated under actual operating condition and has a great influence on the friction process [24]. To address this problem, oxide formation will be studied in a subsequent study, and will be incorporated into the friction coefficient evolution model.

4. Conclusions

The friction coefficient evolution of TiN coating was studied using a ball on disc wear test along with various other characterisation methods. This has enabled a novel interactive friction model to be developed.

1) The ball on disc test results illustrate that the friction evolution process of TiN coating comprises of three stages corresponding to different wear behaviours and mechanisms, namely stage I with low friction, stage II with debris friction, and stage III with coating failure.
2) The wear particles of TiN coating played a very important role in friction and wear process. The initiation of wear particle flow marks the end of stage I with low friction and the start of stage II with high friction, which directly affected the wear life of the TiN coating.
3) The interactive friction model developed in the present research provides an effective approach to model the coating friction and wear, as two interactive responses from a tribo-system. In addition, this model has enabled the description of the friction coefficient evolution and the estimation of wear life of hard coatings. In the subsequent study, further friction and wear experiments of different hard coatings will be performed in order to optimise this model.

Acknowledgements

The strong support from Aviation Industry Corporation of China (AVIC) in this funded research is much appreciated. The research was performed at the AVIC Centre for Structural Design and Manufacture at Imperial College London. In addition, the authors would like to thank colleagues (Xing Liu, Gang Sun and Haibing Zhou) at BAMTRI for providing samples, and express special thanks to Dobre Oana at Imperial College, London for friendly help with friction and wear testing. This work was supported by National Instrumentation grant program of china (Contract No. 2011YQ120039).

References

[1] D.F. Arias, Y.C. Arango, A. Devia, Study of TiN and ZrN thin films grown by cathodic arc technique, Appl. Surf. Sci. 253 (2006) 1683–1690.
[2] A.L. Shao, Y. Cheng, Y. Zhou, M. Li, T.F. Xi, Y.F. Zheng, S.C. Wei, D.Y. Zhang, Electrochemistry properties of multilayer TiN/Ti coatings on NiTi alloy for cardiac occluder application, Surf. Coat. Technol. 228 (2013) 257–261.
[3] X.T. Zeng, S. Zhang, L.S. Tan, Multilayered, (Ti, Al) ceramic coating for high-speed machining applications, J. Vac. Sci. Technol. 19 (2001) 1919–1922.
[4] B. Podgornik, B. Zajec, N. Bay, J. Vižintin, Application of hard coatings for blanking and piercing tools, Wear 270 (2011) 850–856.
[5] B. Podgornik, S. Hogmark, O. Sandberg, Hard PVD coating and their perspectives in forming tool applications, 6th Int. Tool. Conf. 2 (2002) 1053–1065.
[6] E. Bemporad, M. Sebastiani, C. Pecchio, S.D. Ross, High thickness Ti/TiN multilayer thin coatings for wear resistant applications, Surf. Coat. Technol. 201 (2006) 2155–2165.
[7] P. Eh Hovsepian, W.D. Münz, Recent progress in large-scale production of nanoscale multilayer/superlattice hard coatings, Vacuum 69 (2003) 27–36.
[8] S.J. Bull, D.S. Rickerby, The sliding wear of titanium nitride coatings, Surf. Coat. Technol. 41 (1990) 269–283.
[9] K. Kato, Wear in relation to friction — a review, Wear 241 (2000) 151–157.
[10] K. Holmberg, A concept for friction mechanisms of coated surfaces, Surf. Coat. Technol. 56 (1992) 1–10.
[11] D.H. Cho, Y.Z. Lee, Evaluation of ring surfaces with several coatings for friction, wear and scuffing life, Trans. Nonferrous Metal Soc. China 19 (2009) 992–996.
[12] J. Paulitsch, M. Schenkel, A. Schintlmeisterc, H. Hutterc, P.H. Mayrhoferd, Low friction CrN/TiN multilayer coatings prepared by a hybrid high power impulse magnetron sputtering/DC magnetron sputtering deposition technique, Thin Solid Films 518 (2010) 5553–5557.
[13] M. Stoiber, E. Badisch, C. Lugmair, C. Mitterer, Low-friction TiN coatings deposited by PACVD, Surf. Coat. Technol. 163 (4) (2003) 451–456.
[14] K. Holmberg, A. Matthews, Coatings Tribology: Properties, Mechanisms, Techniques and Applications in Surface Engineering, 2nd ed., Elsevier, UK, 2009.
[15] Y.Z. Lee, K.H. Jeong, Wear-life diagram of TiN-coated steel, Wear 217 (1998) 175–181.
[16] J. Denape, J. LamonV., Sliding friction of ceramics: mechanical action of the wear debris, J. Mater. Sci. 25 (1990) 3592–3604.
[17] J.A. Sue, H.H. Troue, Friction and wear properties of titanium nitride coating in sliding contact with AISI 01 steel, Surf. Coat. Technol. 43/44 (1990) 709–720.
[18] S. Wilson, A.T. Alpas, TiN coating wear mechanisms in dry sliding contact against high speed steel, Surf. Coat. Technol. 108–109 (1998) 369–376.
[19] M. Godet, The third-body approach: a mechanical view of wear, Wear 100 (1984) 431–452.
[20] I.L. Singer, How third-body processes affect friction and wear, MRS, Bulletin (1998) 37–40.
[21] N. Fillot, I. Iordanoff, Y. Berthier, Modelling third body flows with a discrete element method—a tool for understanding wear with adhesive particles, Tribol. Int. 40 (2007) 973–981.
[22] N. Fillot, I. Iordanoff, Y. Berthier, Wear modeling and the third body concept, Wear 262 (2007) 949–957.
[23] W.K. Rong, G. Raymond, A. Bayer, D. Peter Engel, C. Sun, Wear of physical vapor deposition TiN coatings sliding against Cr-steel and WC counterbodies, J. Tribol. 120 (1998) 482–488.
[24] I.L. Singer, S. Fayeulle, P.D. Ebnitt, Friction and wear behavior of TiN in air: the chemistry of transfer films and debris formation, Wear 149 (1991) 375–394.
[25] J.F. Archard, Contact and rubbing of flat surfaces, J. Appl. Phys. 24 (1953) 981–988.
[26] J.F. Archard, W. Hirst, The wear of materials under unlubricated conditions, Proc. R. Soc. 236A (1958) 71–73.
[27] J. Takadoum, H. Houmid Bennani, Influence of substrate roughness and coating thickness on adhesion, friction and wear of TiN films, Surf. Coat. Technol. 96 (1997) 272–282.
[28] K. Holmberg, A. Laukkanen, H. Ronkainen, K. Wallin, S. Varjus, J. Koskinen, Tribological contact analysis of a rigid ball sliding on a hard coated surface. Part I: modelling stresses and strains, Surf. Coat. Technol. 200 (2006) 3793–3809.
[29] A.M. Korsunsky, M.R. Mcgurk, S.J. Bull, T.F. Page, On the hardness of coated systems, Surf. Coat. Technol. 99 (1998) 171–183.
[30] K. Komvopoulos, Sliding friction mechanisms of boundary-lubricated layered surfaces. Part II: theoretical analysis, Tribol. Trans. 34 (1991) 281–291.